Associated conference: 5th International Small Sample Test Techniques Conference

Conference location: Swansea University, Bay Campus

Conference date: 10th - 12 July 2018

How to cite: Rouse, J.P., Hyde, C.J., & Kazakeviciute, J. 2018. Investigations into Taylor-Quinney coefficient determination for a 7000 series aluminium alloy using a novel small specimen test technique. *Ubiquity Proceedings*, 1(S1): 42 DOI: https://doi.org/10.5334/uproc.42

Published on: 10 September 2018

Copyright: © 2018 The Author(s). This is an open-access article distributed under the terms of the Creative Commons Attribution 4.0 International License (CC-BY 4.0), which permits unrestricted use, distribution, and reproduction in any medium, provided the original author and source are credited. See http://creativecommons.org/licenses/by/4.0/.

UBIQUITY PROCEEDINGS

ubiquity press open access https://ubiquityproceedings.com

Investigations into Taylor-Quinney coefficient determination for a 7000 series aluminium alloy using a novel small specimen test technique

J. P. Rouse [1*], C. J. Hyde [1] and J. Kazakeviciute [1]

[1]Gas Turbine and Transmission Research Centre (G2TRC), University of Nottingham, UK, NG7 2RD
*****Correspondence: james.rouse@nottingham.ac.uk; Tel.: +44-115-8467-683

Abstract: Thermo-mechanical coupling is a critical component in the thermodynamics of irreversible processes and is related to the dissipation of thermal energy during plastic straining. The Taylor-Quinney coefficient may be thought of as a ratio between thermally dissipated energy and plastic work, thereby giving insight into the thermo-mechanical coupling term. The inclusion of this parameter in a meaningful way is complicated by the various dependencies that the Taylor-Quinney coefficient may be subject to (e.g. loading rate and temperature). Determination of these dependencies is usually achieved through extensive experimentation, wherein temperature variations are monitored (with reference to an unloaded control sample) in a test piece during mechanical loading. There are practical limitations in full size testing methods however, not least relating to the location of full sized control and loaded samples in an environment chamber/furnace while simultaneously maintaining (control sample) temperature uniformity and high resolution temperature measurement (in the loaded sample). The present work details a method based on a novel small specimen testing technique that is currently under development at the University of Nottingham. A small ring of 7175-T7351 aluminum alloy (approximately 10mm in diameter and 2mm in thickness) is loaded between two pins at room temperature, with the local specimen temperature field monitored during monotonic deformation using an infra-red thermal camera. Experimental results are compared for different pin loading rates (namely 0.1mm/s, 1mm/s, and 10mm/s), with particular emphasis placed on localised temperature variations in areas of expected high plasticity. Differences of approximately 0.6°C were observed between 0.1mm/s and 1mm/s tests, with higher temperatures recorded in the latter. Higher temperatures were also noted at small specimen locations associated with localised plasticity. Fundamental thermal material properties are reported for the 7175 alloy in order to facilitate future analysis and heat equation solution efforts (working towards Taylor-Quinney coefficient determination).

Keywords: Small Ring, Taylor-Quinney, Aluminium 7175, Thermoplasticity

1. Introduction

In order to provide a thermodynamic justification for material deformation and damage accumulation models rigorous experimental methods are required which can inform fundamental energy balances. It is well known that, after yield, a potentially large fraction of energy is dissipated as heat. In sufficient circumstances (highly localised high strain rate loadings, for example) this dissipated energy can be observed as a significant change in temperature. The Taylor-Quinney coefficient may be defined as the ratio of energy dissipated as heat during plastic straining to the total plastic work done on the material element. It is the most fundamental material parameter associated with thermoplastic effects, however values are often assumed in the literature without proper experimental justification [1]. In addition to allowing for the more robust thermodynamic formulations of material constitutive equations, representative Taylor-Quinney values (or more aptly, Taylor-Quinney relationships, as multiple dependencies have been experimentally demonstrated in the literature, see section 2) may be used to evaluate plastic dissipation fractions in sophisticated energetic failure criterion (for example, see the work of Daily and Klingbeil in relation to low cycle fatigue crack growth [2] or see Einav et al. [3]). The present work details the use of a small specimen testing technique for the study of the Taylor-Quinney coefficient. An aluminium alloy is used in the present work, however it is expected by the authors that similar techniques could be applied to any material for which the representative volume element is smaller than the small ring geometry. For reference, small rings used in the present work have internal and external radii of 10mm and 11mm, respectively, with a ring thickness of 2mm.

Due to attractive combinations of (relatively) high strength and low density, 7000 series aluminium alloys (such as the 7175-T7351 alloy considered in the present work) have numerous naval, aerospace, and military applications [4–6] and have consequently received a great deal of attention in the literature. In the work of Benoit et al., for example, the microstructure of two 7000 series alloys was analysed, in addition to fundamental mechanical

response parameters such as yield stress, ultimate tensile strength, elongation at fracture, and fracture initiation energy [4]. The orientation of sample forgings and grain size demonstrated no significant influence on yield stress. For 7175 alloys yield strength values of approximately 338+/-8.5MPa were determined. Of particular note was the identification of Zn, Mg, and Cu precipitates, which may act as a hindrances to dislocation motion (thereby providing an important strengthening mechanism). Zn and Mg precipitates were particularly noted for promoting solution strengthening, precipitate strengthening, and stacking fault strengthening mechanisms. 7175-T735 alloys were also studied in the work of Jaya Rao et al. using nonlinear ultrasonic non-destructive methods [7]. Samples with prior plastic straining were analysed, with resulting NLU parameter variations suggesting two stage dislocation process in the material's deformation behaviour. Wen et al.'s work focused on the effects of various ageing treatments on the texture/microstructure of high Zn content aluminium alloys, particularly through the determination of hardness, electrical conductivity, and basic mechanical material properties [5]. Transmission electron microscopy (TEM) was also used to investigate precipitates geometric characteristics and mismatches with the matrix material. Rapid reductions in yield stress, ultimate tensile strength, and hardness were observed with exposure time for ageing processes at 160°C, with approximate values for high Zn content precipitate size and spacings in the range of 2-7nm and 7-13nm, respectively. Similar results, along with phenomenological model developments, are reported in the work of Lam Wing Cheong et al. for 7175-T7351 alloys [8].

The influence of Cu rich precipitates on extrusion characteristics of aluminium alloys was investigated by Paulisch and co-workers through examination of 7108 (which is Cu free) and 7175 [9]. Extrusions performed with 7108 could be made with a wide range of parameters and resulting strands were crack free (the ultimate tensile strength after ageing was estimated as 426MPa). Conversely, 7175 extrusions speeds were limited as frictional heating (potentially generating temperatures of 525°C) led to the formation of eutectic AlMgZnCu phase. 7175 extrusion strands displayed hot cracks, however great improvements in ductility were noted through reductions in dislocation density and enhanced dynamic recovery. Ultimate tensile strength values of 636MPa were determined. Paulisch and co-workers also investigated natural ageing in 7020 and 7175 alloys by monitoring samples at room temperature over an 18 month period. Two phases, namely Al2CuMg and Al12Mg2Cr2, were identified in 7175 as being potentially hazardous due to the capacity for remelting. Fe rich particles in 7020 were not influenced by repeat annealing. Langille et al. noted a break down in the commonly assumed linear relationship between fracture strain and yield stress in AA6063 for samples which were plastically pre-strained prior to ageing [10]. Linear relationships could however be recovered when dislocation spacing is considered in formulations. Goueffon and co-workers examined coefficients of thermal expansion in anodised 7175 films for space applications using 10mm thick beam bending experiments (values of $13.0+/-1.0x10^{-6}K^{-1}$ were suggested [6]), with values being relatively independent of the porosity of the film [11].

The present work describes a small specimen method which is suitable for the investigation of the Taylor-Quinney coefficient. The small ring test was originally proposed by Hyde and Sun as a high sensitivity method for the study of primary and steady state creep [12]. Large (by small specimen standards) gauge lengths of approximately 50mm were noted for modest levels of total deformation, however it must be noted that gauge length is a function of total ring deflection. For nominally constant load creep tests (equivalent to traditional full sized uniaxial tests) adaptive loading must be implemented to account for this [13]. The small ring test set-up is summarised in figure 1 (showing both undeformed and deformed specimen states). A ring is loaded by two pins (allowing for self-alignment and a minimal influence of friction on the specimen response) such that it may elongate. In creep tests, a constant load P is applied and deflection of the pins is monitored. Tensile (imposed constant deflection rate) small ring tests are performed in the present work at room temperature, with specimen surface temperatures monitored in order to observe thermoplastic effects. P is recorded for changes in pin displacement (Δ-Δ_0). To the authors' knowledge, this is the first instance of a small specimen being used for this type of study.

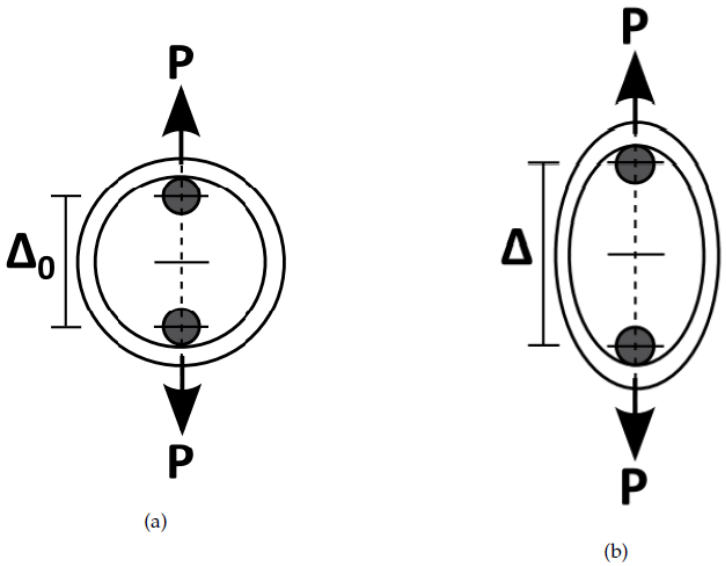

Figure 1. A schematic of the small ring testing method, showing (a) undeformed and (b) deformed specimens.

2. An Overview of Thermoelastic and Thermoplastic Phenomenon

Heat transfer associated with material straining has received a good deal of attention in the literature, however Rittel has noted that the Taylor-Quinney coefficient (the most fundamental parameter associated with thermoplastic effect, which is particularly important in impact analyses [14]) values are often assumed to be 0.9 [1]. Dependencies on factors such as loading rate have been experimentally demonstrated, yet resulting relationships are often neglected in otherwise detailed simulations. The Taylor-Quinney coefficient (β) may be expressed by equation (1), where $\dot{q}_P$ is the (specific) power dissipated as heat (due to irreversibilities associated with plasticity or damage, for example) and $\dot{w}_P$ is the (specific) plastic power [15]. Note lower case terms used in this section relate to specific quantities. It is of course easy to show that the fraction of stored energy, η, is related to β by η=1-β [16]. Care must however be taken when defining β. As pointed out by Rittel [17], power quantities are considered in equation (1) (rate terms, such as those related to the heat and work quantities q_P and w_P, are here denoted by a dot). The "integral" form of β (here defined at β_{int} and related to a time period t) can be expressed as equation (2), allowing for the relationship between β and β_{int} given in equation (3) to be developed [18].

$$\beta = \frac{\dot{q}_P}{\dot{w}_P} \tag{1}$$

$$\beta_{int} = \frac{q_P}{w_P} = \frac{1}{w_P}\int_0^t \beta \dot{w}_P d\tau \tag{2}$$

$$\beta = \beta_{int} + \frac{w_P}{\dot{w}_P}\dot{\beta}_{int} \tag{3}$$

The determination of β for polymer materials has received particular attention in the literature. Shao et al. considered the glassy polymers polycarbonate (PC) and polymethyl methacrylate (PMMA) and showed, using material models which accounted for strain hardening and softening, that β can vary between approximately 0.5 and 0.8 (based on plastic strain magnitude and loading rate) [14]. Maurel-Pantel and co-workers investigated semi-crystalline polyamide 66 (PA66) using digital image correlation (DIC) and infra-red imaging techniques (to evaluate total strain and thermal field parameters, respectively) at multiple tensile strain rates, namely 0.1/s, 0.01/s, and 0.001/s [19]. A difference in peak temperature of 15°C was noted between different loading rate results, with similar observations for shear tests. Constitutive relations used in this work were based on Billon [20]. PA66 was also studied by Benaarbia et al. for low cycle fatigue conditions [21]. Cycle by cycle evaluations of β highlighted hot spots in dissipation fields and a range of values (from 0.4 to 0.8) were noted (over approximately 7000 loading cycles). Due to the importance of β in high strain rate problems (such as impact), split-Hopkinson (or Kolsky) bars have been used in several experimental studies. The dependence of dynamic loading mode on β was studied by Rittel, for example, and potentially large fluctuations correlated with loading mode for certain materials (e.g.

annealed commercially pure Titanium, grade 2) [1]. Similar work was conducted by Galán et al. for Ti6Al4V [22] and Jovic et al. for 304L stainless steel and 5754 aluminium alloy [23]. A strong dependence on strain rate was noted in the work of Fekete for 15Ch2MFA (bainitic structure with fine grains) reactor steel, although 08Ch18N10T (austenitic structure with coarse grains) showed negligible levels of loading rate dependency [16]. Multi-phase (Martensite and Austenite) 304 stainless steel materials were analysed by Zaera [24]. This work highlighted that phase transformation mechanisms can release latent heat, leading to experimental observations where β takes a value greater than unity. Polycrystalline aluminium was investigated by Badulescu, with a relationship between β and grain orientation suggested [25].

It is worth noting here (in order to assist discussion later in the present work) that the measurement small temperature changes on the surface of components/specimens has been used for many years to evaluate stress fields. Such techniques are generally known as thermoelastic stress analysis methods and commonly require that material samples are cycled at such a rate that conduction can be neglected [26]. A general expression for the temperature change associated with thermoelastic mechanisms is given in equation (4), where T is the observed temperature, ρ is the material density, C_ε is the specific heat capacity at constant strain, σ_{ij} is a component of the symmetric stress tensor, ε_{ij} is a component of the symmetric total strain tensor, and Q is an input heat. If conduction is neglected, plane stress conditions assumed, and it is reasonable to consider parameters such as Young's modulus and Poisson's ratio (E and υ, respectively) independent of temperature, equation (4) may be simplified and rearranged to give equation (5), which can relate measured temperature fluctuations to stress state. Note that C_ε may be related to the specific heat capacity at constant pressure (C_P) by equation (6) (where α is the coefficient of thermal expansion) and that $\alpha/\rho C_P$ is often referred to as the thermoelastic constant. Thermodynamic justification for thermoelastic effects (and importantly equation (4)) is based on the assumption of reversibility in elastic deformation [27]. The Helmholtz free energy (φ) may be defined as the internal energy (u, a function of temperature and total strain) less the product of temperature (T) and entropy (s), or φ=u-Ts. Recalling the first and second laws of thermodynamics and evaluating specific heat and work contributions, an expression for the increment in entropy may be found such that equation (4) can be derived [27].

$$\Delta T = \frac{T}{\rho C_\epsilon}\Sigma\frac{\partial \sigma_{ij}}{\partial T}\epsilon_{ij} + \frac{Q}{\rho C_\epsilon} \text{ for } i,j = 1,2,3 \tag{4}$$

$$\Delta T = -\frac{\alpha}{\rho C_P} T \sum_{i=1,2} \sigma_{ii} \tag{5}$$

$$C_\epsilon = C_P - \frac{2E\alpha^2 T}{\rho(1-\nu)} \tag{6}$$

In irreversible processes, such as plastic deformation, there is always an increase in entropy [27]. The definition of Helmholtz free energy presented above (φ=u-Ts) is still valid, however it is important to note that in the elastic-plastic case internal energy is a function of state variables related to, for example, kinematic and isotropic hardening (allowing for the quantification of plastic strain) in addition to the elastic strain component and temperature (as was assumed in the thermoelastic case). The Clausius-Duhem inequality expresses the second law of thermodynamics in a way which is convenient for continuum mechanics study and may be represented by equation (7), where $\dot{\boldsymbol{\sigma}}$ and $\dot{\boldsymbol{\varepsilon}}$ are the stress and strain rate tensors, respectively, and $\dot{q}$ is a heat flux. Equation (7) quantifies a total dissipation (d), which may be decomposed into a mechanical (also known as intrinsic) component (d_m, see equation (8), which is equivalent to the quantity $\dot{q}_P$ referenced in equation (1)) and a thermal component (d_{th}, see equation (9)), such that $d=d_m+d_{th}$ [28]. Note that the former is related to irreversibilities which cause a change in the material's microstructure (plasticity, for example) and the latter is related to the existence of a temperature gradient across the material. In order to experimentally evaluate d_m ($=\dot{q}_P$) the heat equation must be solved (equation (10)). Note that mechanical dissipation may be decomposed into thermomechanical coupling and dissipative components. Thermomechanical contributions have been neglected in some studies [21], however evaluation may be related in some cases to thermoelastic power [15].

$$d = \dot{\psi} + s\dot{T} - \frac{1}{\rho}\boldsymbol{\sigma} : \dot{\boldsymbol{\epsilon}} + \frac{\dot{q}.\nabla T}{\rho T} \leq 0 \tag{7}$$

$$\delta_m = \dot{q}_P = \frac{1}{\rho}\boldsymbol{\sigma} : \dot{\boldsymbol{\epsilon}} - \dot{\psi} - s\dot{T} \tag{8}$$

$$\delta_{th} = -\frac{\dot{q}.\nabla T}{\rho T} \tag{9}$$

$$\rho C_P \frac{\partial T}{\partial t} - \nabla.(k\nabla T) = \delta_m = \dot{q}_P \tag{10}$$

Multiple excellent review articles have been published on thermoplastic effects from both theoretical and experimental perspectives. Interested readers are directed to the work of Bertram and Krawietz [28], Knysh and Korkolis [18], Einav et al. [3], and Pottier et al. [15].

3. Experimental Setup

Small ring testing is completed here using a Tinius-Olsen H25KS test rig (see figure 2 (a)). Load is transferred from the machine end grips to the small ring sample through a modified Nimonic alloy test specimen (see figure 2 (b)) which also locates Nimonic loading pins. Pin displacement is recorded through LVDTs connected to knife edge ridges on the modified Nimonic test specimen. The Young's modulus of Nimonic is approximately three times greater than that of aluminium. Consequently, the stiffness of the ring test specimen is assumed to be significantly less than the stiffness of the modified "grip" sample, suggesting that LVDT measurements are approximately equivalent the to the pin displacements. Three loading rates (namely 0.1mm/s, 1mm/s, and 10mm/s) are applied here in order to indicate any rate dependencies for the 7175 material and alter the time scales for heat transfer.

Temperature fields are monitored using a FLIR SC7200 infra-red thermal camera. A thermal calibration curve for the high magnification camera lens used in the present work was established by relating thermocouple readings to measured digital levels. Diurnal variations in laboratory ambient temperature were used to generate a range of data points (see figure 3). A linear correlation is used in the present work, allowing for the evaluation of temperatures (T) based on camera digital level (X) using the function $T = 6.745\text{x}10^{-3}X - 11.480$. Note that two independent tests were performed for each loading rate, thereby allowing temperature fields to be monitored during deformation on "front" (as shown in figure 1) and "side" projections of the small ring sample. Example temperature field plots for both of these projections and all loading rates are given in figure 4. Temperature fields were sampled at 100Hz in the 0.1mm/s and 1mm/s tests and at 200Hz in the 10mm/s tests.

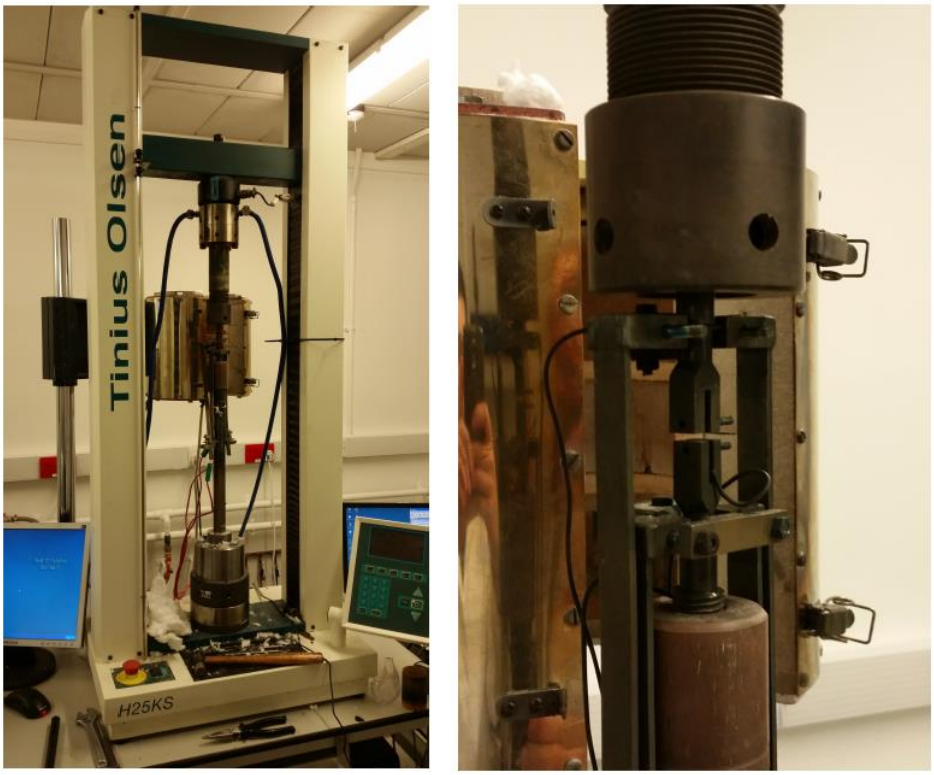

Figure 2. The Tinius-Olsen H25KS test rig used for small ring testing in the present work, showing **(a)** the general experimental setup and **(b)** a close up of the modified small ring specimen grips.

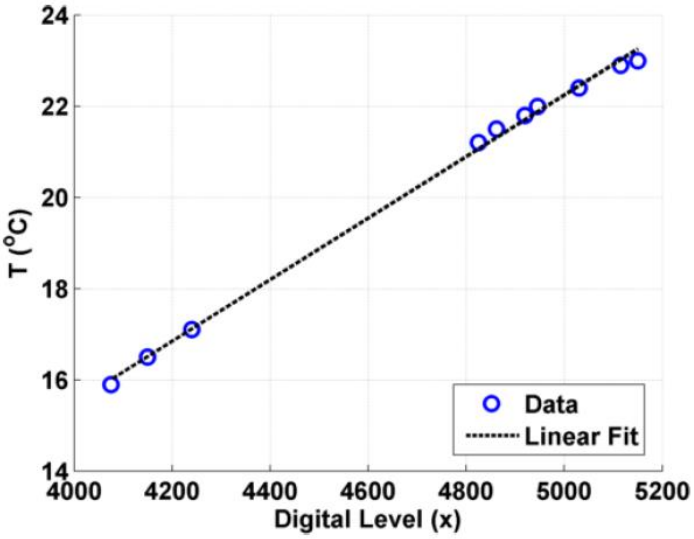

Figure 3. The thermal calibration curve used in the present work, used to correlate thermal camera digital levels and temperature.

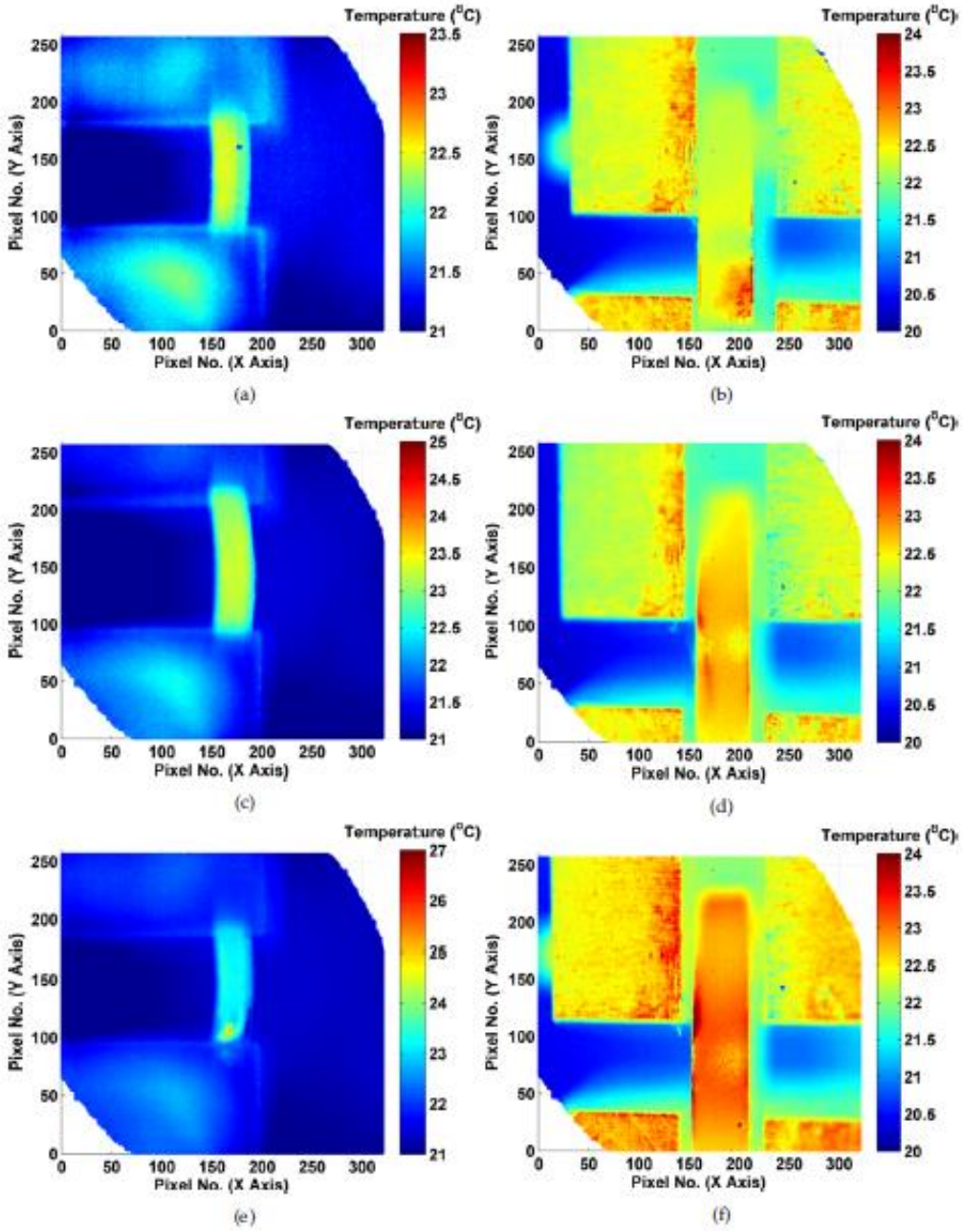

Figure 4. Example temperature field plots, shown for 'front' and 'side' projections for 0.1mm/s ((a) and (b)), 1mm/s ((c) and (d)) and 10mm/s ((e) and (f)) loading rates.

4. Thermal Parameter Determination

In order to investigate thermoplastic effects (and consequently estimate Taylor-Quinney coefficients) it is necessary to solve the heat equation. Thermal source terms related to plastic straining must be balanced with losses to the testing environment (by natural convection, for example) in order to approximate the dynamic temperature field. Fundamental thermal properties of 7175-T7351 aluminium are explored here in order to facilitate future heat transfer analyses. Specific heat capacity was estimated using a Netzsch DSC 204 HP Differential Scanning Calorimeter. Tests were performed at ambient conditions. Variations in specific heat capacity were observed over a 5 hour period in order to determine the stability of the results. Only minor variations were observed over this sampling period. A mean value of 864.40J.kg^{-1}.K^{-1} is suggested here.

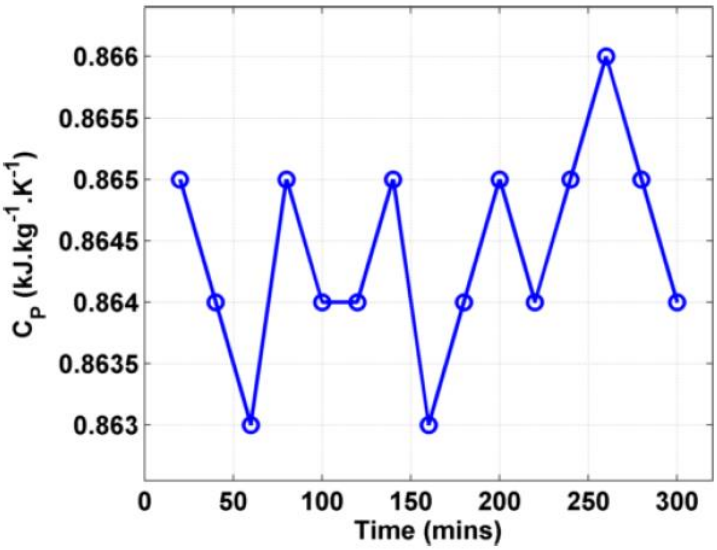

Figure 5. Variations in specific heat capacity (C_p) recorded over 5 hours.

The Wiedemann-Franz law is used in the present work in order to estimate thermal conductivity based on electrical conductivity measurements. The Wiedemann-Franz law may be expressed in the form shown in equation (11), where κ is thermal conductivity, σ_E is electrical conductivity, T is instantaneous temperature (here assumed to be 273K, representative of typical laboratory ambient temperatures), and L is the Lorenz number (here taken to be $2.44x10^{-8}$W.Ω.K^{-2}) [29]. Four point direct current potential drop tests were performed using 4 injection current levels on a 0.03m by 0.072m by 0.6m bar of the 7175 material. Results are presented in table 1. Difficulties in reading small potential drops are suggested for the apparent dependency of thermal conductivity on injection current observed in table 1, therefore a value of 190.04W.m^{-1}.K^{-1} is recommended here (being the average of the "stabilised" 2.5A and 3A results).

$$\frac{K}{\sigma_E} = LT \tag{11}$$

Table 1. A summary of four point potential drop test results performed on 7175 and resulting thermal conductivity estimations (based on the Wiedemann-Franz law, see equation (11)).

Current (A)	Potential Drop (μV)	Resistance ($\mu\Omega$)	Electrical Resistivity ($\Omega.m$)	Electrical Conductivity ($S.m^{-1}$)	Thermal Conductivity ($W.m^{-1}.K^{-1}$)
1	9.5	9.5	$3.42x10^{-8}$	$29.24x10^{6}$	209.04
2	20	10	$3.60x10^{-8}$	$27.78x10^{6}$	198.59
2.5	26	10.4	$3.74x10^{-8}$	$26.71x10^{6}$	190.95
3	31.5	10.5	$3.78x10^{-8}$	$26.46x10^{6}$	189.13

Density for the 7175 material was estimated using a MicroMetrics Accupyc 1330 pycnometer. 10 successive runs (purges) were performed on a 19.1867g sample. A mean density value of 2.7581g.cm^{-3} was found, with a peak deviation from mean of 0.0487%.

5. Results

Conventional (full size) monotonic testing of 7175 at room temperature has suggested minimal time dependency in the constitutive behaviour. Results presented in figure 6, which show the relationship between pin load and displacement, support this observation for the 0.1mm/s and 1mm/s results. A remarkable level of repeatability (in terms of initial linear and non-linear material behaviour) should be noted in all observations made here; this directly follows from the self-aligning nature of the small ring specimen and the negligible influence of friction on the recorded specimen response. Further evidence of specimen response repeatability can be seen in the time series plots shown in figure 7. A clear deviation in the specimen response is observed in the 10mm/s data sets

(see figures 6 and 7). Possible explanations for the alternative specimen behaviours are discussed in section 6. At presents, readers are requested to note that, in the 0.1mm/s and 1mm/s results, non-linearity appears to commence at pin loads of approximately 150N. From figure 7, this pin load can be related to test times of 3.5s and 0.4s for the 0.1mm/s and 1mm/s cases, respectively.

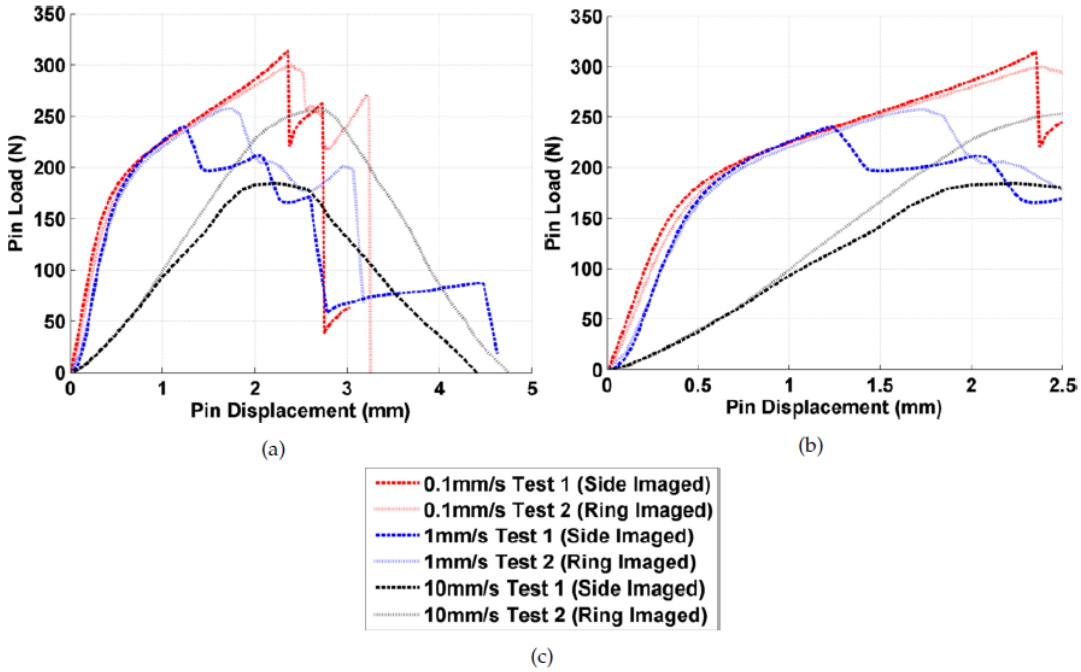

Figure 6. Pin load /displacement relationships observed for the three loading rates (0.1mm/s, 1mm/s and 10mm/s) used in the present work (note that repeat results are denoted by the temperature field imaging orientation, namely 'front' and 'side'). Full load/displacement curves are shown in **(a)** with elastic/plastic behaviour highlighted in **(b)** (a figure legend is presented in **(c)**).

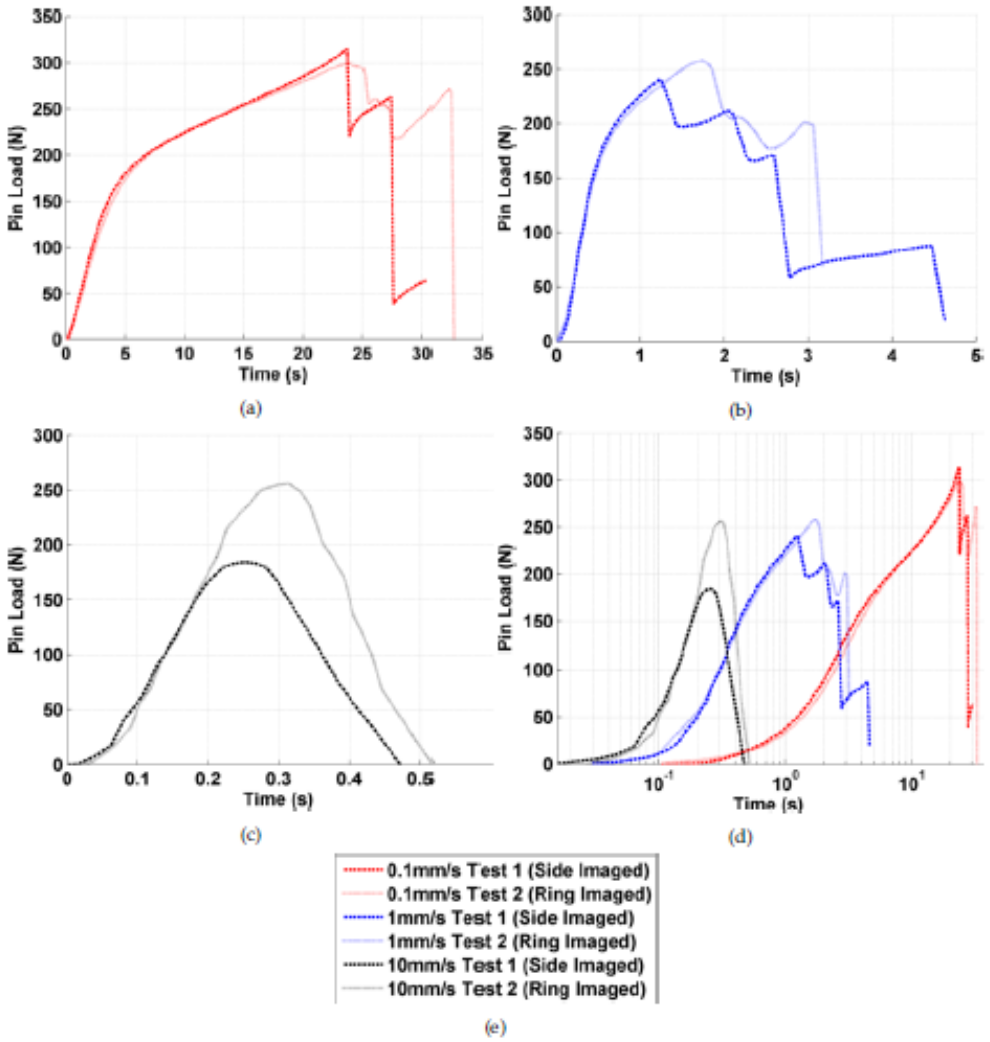

Figure 7. Pin load /time relationships observed for the three loading rates (0.1mm/s, 1mm/s and 10mm/s) used in the present work (note that repeat results are denoted by the temperature field imaging orientation, namely 'front' and 'side'). Full load/time curves are shown in **(a), (b),** and **(c)** (relating to loading rates 0.1mm/s, 1mm/s and 10mm/s respectively). Logarithmic time series are used in **(d)** to compare the three loading rate results. A figure legend is presented in **(e)**.

Temperature variations for various time instants in the small ring tests are presented in figures 9 to 11 (for the 0.1mm/s, 1mm/s, and 10mm/s, respectively). Figure 8 indicates the locations of sampling paths for front and side projections of the ring. In both cases, sampling is conducted from left to right (as shown in figure 8). Bespoke Matlab scripts have been developed to allow the user to track the ring as it deforms. Consequently, the paths presented in figure 8 are assumed to translate with the deforming small ring specimen. It is however important to note that, as the sampling paths are located on planes of symmetry in the specimen, they are assumed to remain planar. Generally speaking, uniform temperature profile are observed through the specimen thickness (side projections, or (b) sub-figures below), with the magnitude of this temperature increasing with test time. For front projections, higher temperatures are noted at the internal ring surface. Anomalies such as the large increase in temperature observed to the right hand side of figure 9 (b) associated here with the onset of failure and non-uniform contact (finite element simulation of the small ring has indicated a relaxation of contact pressure at the edges of the sample during loading). Future work will look to investigate this further.

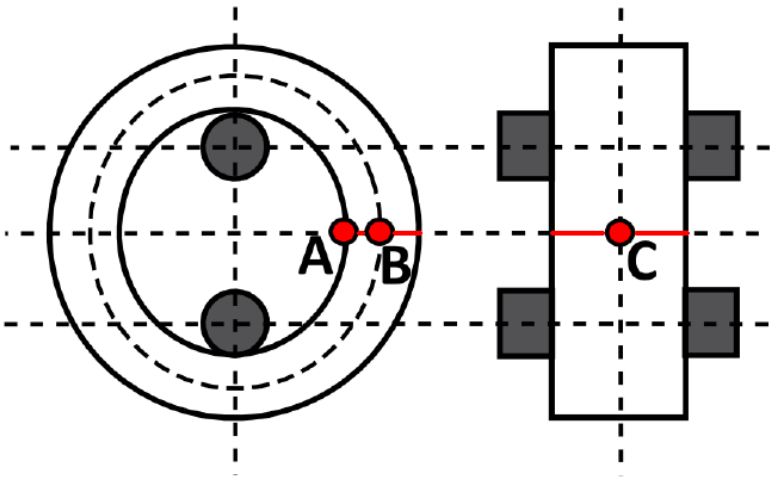

Figure 8. Sampling paths and points used for examination of temperature fields in the small ring samples.

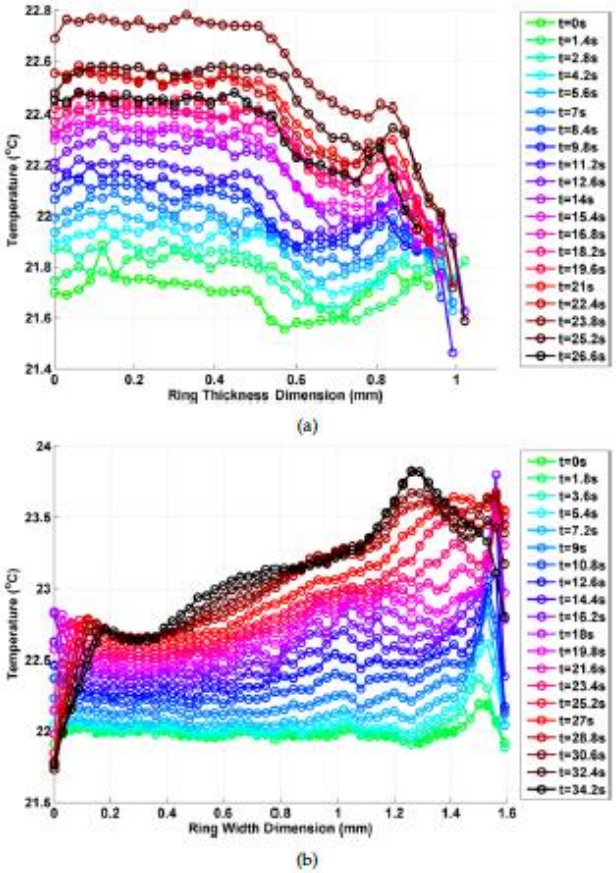

Figure 9. Temperature distribution variations (with test time) along the paths defined in figure 8, showing **(a)** front and **(b)** side projections for the 0.1mm/s loading case.

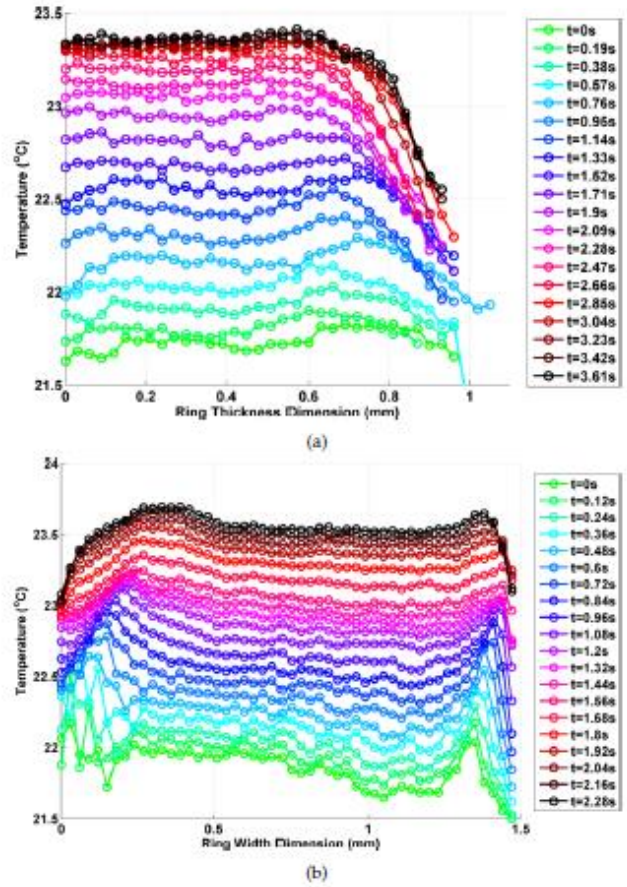

Figure 10. Temperature distribution variations (with test time) along the paths defined in figure 8, showing **(a)** front and **(b)** side projections for the 1mm/s loading case.

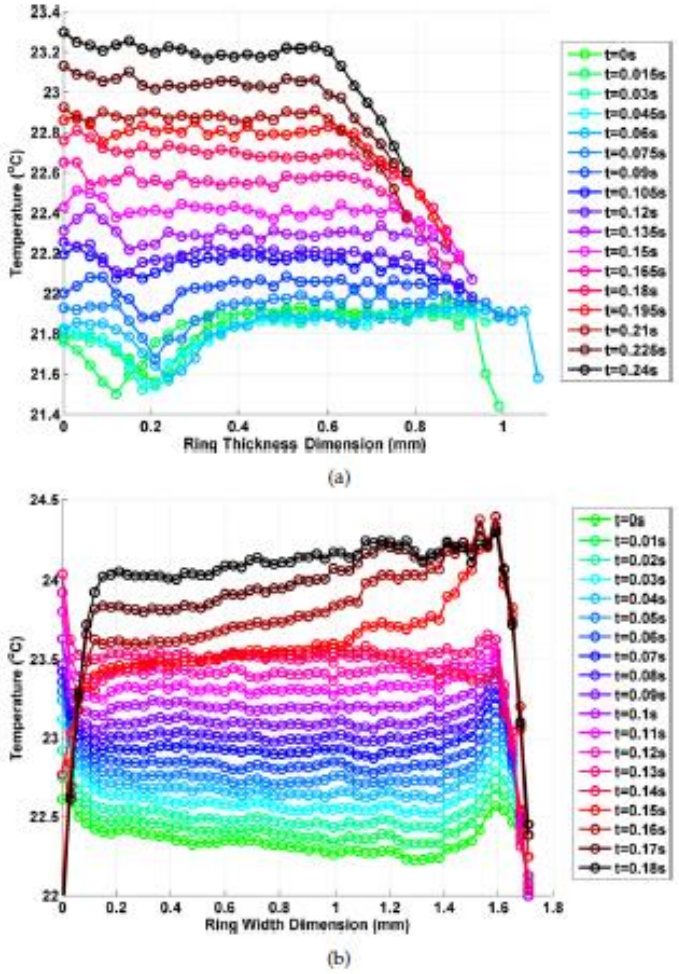

Figure 11. Temperature distribution variations (with test time) along the paths defined in figure 8, showing **(a)** front and **(b)** side projections for the 10mm/s loading case.

6. Discussion and Conclusions

A small ring tensile testing technique has been employed in order to investigate thermoplastic effects in 7175-T7351 aluminium alloy. Highly localised regions on plasticity (at the inside ring surface perpendicular to the loading direction) combined with very small volumes of material in the specimen were expected to develop characteristic temperature fields, thereby resulting in a sensitive testing method suitable for the study of the Taylor-Quinney coefficient. Indeed, front projections in figures 9 to 11 indicate higher temperature profiles at the internal ring surface, as expected. Figure 12 displays temperature changes associated with the sampling locations identified in figure 8 (A, B, and C) and, in the case of the 0.1mm/s and 1mm/s data, 1mm/s temperature profiles are approximately 0.6°C greater than 0.1mm/s profiles prior to failure. It is important to note that, in figure 11, temperature changes have been corrected for variations in ambient temperature by monitoring grip temperature fields (which are almost entirely uniform) throughout the test. Temperature changes associated with the 10mm/s data do not confirm with the expected trend. Even if no rate dependency in the Taylor-Quinney coefficient is assumed for 7175, a reduction in time scales over which heat transfer may take place (resulting from the faster loading rate) would suggest more localised and higher magnitude temperature fields. The thermal parameters determined in section 4 may be used to explore this point further through evaluation of 7175's thermal diffusivity ($7.97 \times 10^{-5} m^2.s^{-1}$). Taking a characteristic length of 1mm (the thickness of the small ring specimen), a diffusive characteristic time of 79.71s may be determined. Given that all test durations are less that this value (see figure 7), local temperature field features are justifiably expected. As noted previously, the linear and non-linear regions observed in force/displacement plots (see figure 6) for the 0.1mm/s and 1mm/s tests are not observed in the 10mm/s tests. A potential explanation for this can be derived by observing the initial non-linearity in the 1mm/s force/displacement curve (figure 6 (b)). The small ring specimen is in contact with two loading pins. It is assumed that local deformation around these pins does not

significantly contribute to the overall deformation of the specimen (the ring being intrinsically flexible upon first loading). At high strain rates however, it is suspected that this is not the case. Note that, based on a representative gauge length of 50mm, the strain rates associated with loading rates of 0.1mm/s, 1mm/s, and 10mm/s are 0.2%/s, 2%/s, and 20%/s, respectively. The latter of these is noted as being particularity high and may represent a limit for the small ring test in its current form. Future work will look to test intermediate strain rates in order to support this claim.

Some evidence of thermoelastic effects may be observed in the results presented here. Temperature changes associated with the linear region of the specimen force/displacement response are generally small (note that profiles in figures 9 and 10 are of similar magnitude before 3.5s and 0.4s for the 0.1mm/s and 1mm/s results, respectively). Furthermore, drops in temperature may be observed at the beginning of the tests in figure 12. The non-cyclic nature of the tensile small ring test makes further examination of these effects difficult (conditions close to adiabatic have clearly not been achieved), however the results discussed here indicate a potential focus for future work.

The experimental technique employed here appears to β suitable for the determination of the Taylor- Quinney coefficient at modest strain rates. Very good levels of repeatability and the small amounts of source material used have the potential to make small ring tensile tests an effective and efficient to study some of the various dependencies associated with β. As with full sized samples failure is less repeatable (see figure 6) and it is unclear at present how sensitive these results are to tolerances in the specimen design. Localised plasticity has allowed for temperature changes to 1.7°C to be observed, resulting from intrinsic material dissipation. Small specimens hold a further advantage over full sized equivalents in this field of study. It is reasonably easy to mount several in a furnace simultaneously, allowing for the investigation of β at temperature (with one unloaded sample acting as a reference for environmental temperature control). The isolation of noise in results of this type is a problem that plagues all testing (full sized or small), however the highly localised nature of plasticity in the small ring specimen may offer a solution to this in the future.

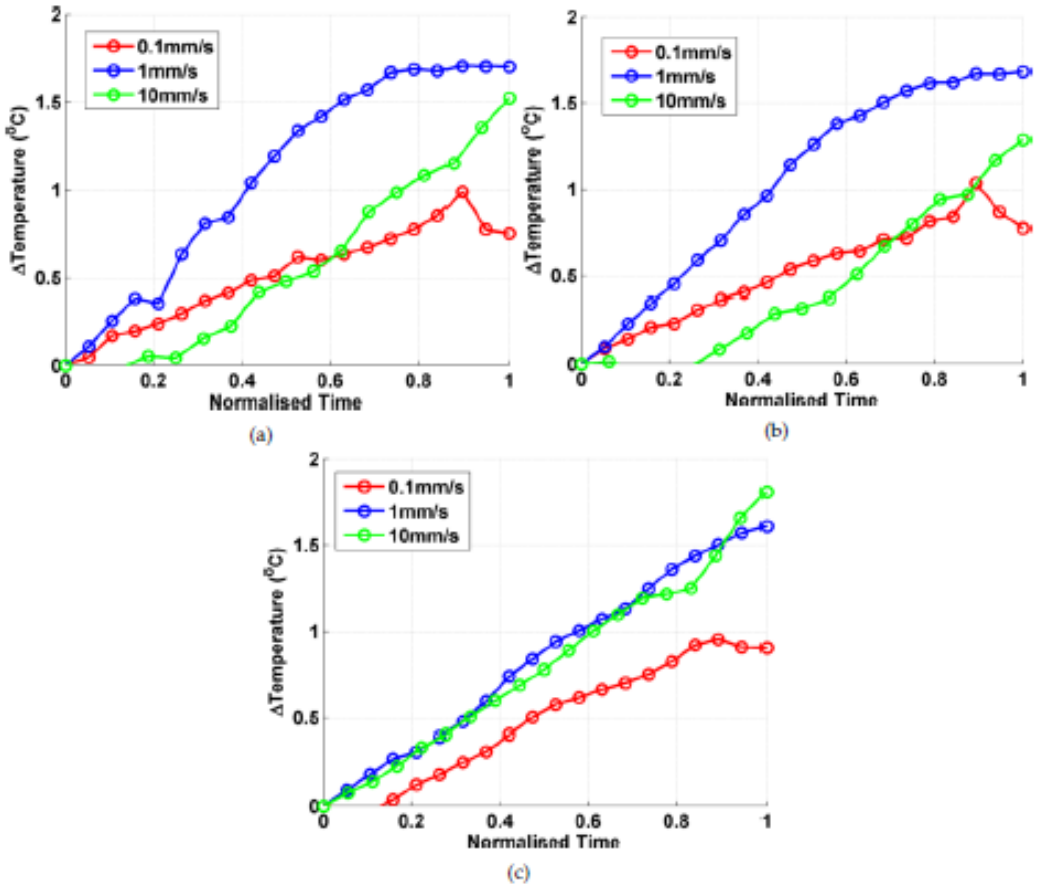

Figure 12. Observed temperature changes in sampling locations **(a)** A, **(b)** B and **(c)** C (see figure 8) for the three loading rates applied in the present work.

References

1. Rittel D.; Zhang L.H.; Osovski S. The dependence of the Taylor-Quinney coefficient on the dynamic loading mode. Journal of the Mechanics and Physics of Solids. 2017;107:96–114.
2. Daily J.S.; Klingbeil N,W. Plastic dissipation in fatigue crack growth under mixed-mode loading. International Journal of Fatigue. 2004;26:727–738.
3. Einav I.; Houlsby G.T.; Nguyen G.D. Coupled damage and plasticity models derived from energy and dissipation potentials. International Journal of Solids and Structures. 2007;44:2487–2508.
4. Benoit S.G.; Chalivendra V.B.; Rice M.A.; Doleski R.F. Characterisation of the microstructure, fracture, and mechanical properties of aluminium alloys 7085-O and 7175-T7452 hollow cylinder extrusions. Metallurgical and Materials Transactions A. 2016;47A:4476–4483.
5. Wen J.; Fan Y.; Wang G.; Jin L.; Li X.; Li Z.; et al. Aging behavior and precipitate characterization of a high Zn-containing Al-Zn-Mg-Cu alloy with various tempers. Materials & Design. 2016;101:16–23.
6. Goueffon Y.; Mabru C.; Labarrére M.; Arurault L.; Tonon C.; Guigue P. Mechanical behaviour of black anodic films on 7175 aluminium alloy for space applications. Metal Finishing. 2010;108:22–27.
7. Jaya Rao V.V.S.; Kannan E.; Prakash K.R.; Balasubramaniam. V. Observation of two stage dislocation dynamics from nonlinear ultrasonic response during the plastic deformation of AA7175-T7351 aluminium alloy. Materials Science and Engineering: A. 2009;512:92–99.
8. Lam W.; Cheong M.F.; Rouse J.P.; Hyde C.J.; Kennedy A.R. The prediction of isothermal cyclic plasticity in 7175-T7351 Aluminium alloy with particular emphasis on thermal ageing effects. International Journal of Fatigue, https://doi.org/10.1016/j.ijfatigue.2018.05.010.
9. Paulisch M.C.; Lentz M.; Wemme H.; Andrich A.; Driehorst I.; Reimers W. The different dependencies of the mechanical properties and microstructures on hot extrusion and artificial aging processing in case of the alloys Al 7108 and Al 7175. Journal of Materials Processing Technology. 2016;233:68–78.
10. Langille M.R.; Diak B.J.; Saimoto S. Re-examining the relation between fracture strain and yield stress in Al-Mg-Si alloys. Materials Science and Engineering: A. 2017;705:196–199.
11. Goueffon Y.; Mabru C.; Labarrére M.; Arurault L.; Tonon C.; Guigue P. Investigations into the coefficient of thermal expansion of porous films prepared on AA7175 T7351 by anodizing in sulphuric acid electrolyte. Surface and Coatings Technology. 2010;205:2643–2648.
12. Hyde T.H.; Sun W. A novel, high-sensitivity, small specimen creep test. Journal of Strain Analysis for Engineering Design. 2009;44:171–185.
13. Hyde C.J.; Hyde T.H.; Sun W. Small ring testing of high temperature materials. Key Engineering Materials. 2017;734:168–175.
14. Shao G.; Zhu S.; Wang Y.; Zhao Q. An internal state variable thermodynamic model for determining the Taylor-Quinney coefficient of glassy polymers. International Journal of Mechanical Sciences. 2017;126:261–269.
15. Pottier T.; Toussaint F.; Louche H.; Vacher P. Inelastic heat fraction estimation from two successive mechanical and thermal analyses and full-field measurements. European Journal of Mechanics - A/Solids. 2013;38:1–11.
16. Fekete B.; Szekeres A. Investigation on partition of plastic work converted to heat during plastic deformation for reactor steels based on inverse experimental-computational method. European Journal of Mechanics - A/Solids. 2015;53:175–186.
17. Rittel D. On the conversion of plastic work to heat during high strain rate deformation of glassy polymers. Mechanics of Materials. 1999;31:131–139.
18. Knysh P.; Korkolis Y.P. Determination of the fraction of plastic work converted into heat in metals. Mechanics of Materials. 2015;86:71–80.
19. Maurel-Pantel A.; Baquet E.; Bikard J.; Bouvard J.L.; Billon N. A thermo-mechanical large deformation constitutive model for polymers based on material network description: Application to a semicrystalline polyamide 66. International Journal of Plasticity. 2015;67:102–126.
20. Billon N. New constitutive modelling for time-dependent mechanical behaviour of polymers close to glass transition: Fundamentals and experimental validation. Journal of Applied Polymer Science. 2012;125:4390–4401.
21. Benaarbia A.; Chrysochoos A.; Robert G. Kinetics of stored and dissipated energies associated with cyclic loadings of dry polyamide 6.6 specimens. Polymer Testing. 2014;34:155–167.

22. Galán J.; Verleysen P.; Degrieck J. Thermal Effects During Tensile Deformation of Ti-6Al-4V at Different Strain Rates. Strain. 2013;49:354–365.
23. Jovic C.; Wagner D.; Herve P.; Gary G.; Lazzarotto L. Mechanical behaviour and temperature measurement during dynamic deformation on split Hopkinson bar of 304L stainless steel and 5754 aluminium alloy. Journal de Physique IV. 2006;134:1279–1285.
24. Zaera R.; Rodríguez-Martínez J.A.; Rittel D. On the Taylor-Quinney coefficient in dynamically phase transforming materials. Application to 304 stainless steel. International Journal of Plasticity. 2013;40:185–201.
25. Badulescu C.; Grédiac M.; Haddadi H.; Mathias J.D.; Balandraud X.; Tran H.S. Applying the grid method and infrared thermography to investigate plastic deformation in aluminium multicrystal. Mechanics of Materials. 2011;43:36–53.
26. Dulieu-Barton J.M. Introduction to thermoelastic stress analysis. Strain. 1999;35:35–39.
27. Pitarresi G.; Patterson E.A. A review of the general theory of thermoelastic stress analysis. The Journal of Strain Analysis for Engineering Design. 2003;38:405– 417.
28. Bertram A.; Krawietz A. On the introduction of thermoplasticity. Acta Mechanica. 2012;223:2257–2268.
29. Jones W.; March N.H. Theoretical Solid State Physics. Dover Publishing; 1986.